Clay Minerals, (2015) **50**, 417–430

Zn-rich smectite from the Silver Coin Mine, Nevada, USA

S. KAUFHOLD[1,*], G. FÄRBER[2], R. DOHRMANN[1,3], K. UFER[1] AND G. GRATHOFF[4]

[1] *BGR, Bundesanstalt für Geowissenschaften und Rohstoffe, Stilleweg 2, D-30655 Hannover, Germany*
[2] *Bornsche Str. 9, D-39326 Samswegen, Germany*
[3] *LBEG, Landesamt für Bergbau, Energie und Geologie, Stilleweg 2, D-30655 Hannover, Germany*
[4] *Ernst-Moritz-Arndt Universität Greifswald, Institute für Geographie und Geologie, Friedrich-Ludwig-Jahn-Str. 17a, D-17487 Greifswald, Germany*

(*Received 20 July 2014; revised 1 June 2015; Associate Editor: Helge Stanjek*)

ABSTRACT: More than 100 minerals have been reported from the Silver Coin Mine, Nevada USA; five new minerals have been discovered here, due to the unusual geochemical environment. The present study reports on the investigation of a greenish clayey sample from the Silver Coin Mine. After the separation of a fine fraction to enrich the clay minerals, sauconite, a rare Zn-rich smectite, was found by X-ray diffraction (XRD) and was further characterized by differential thermal analysis (DTA), infrared (IR) spectroscopy and scanning electron microscopy (SEM). The Zn-rich smectite is accompanied by illite, minor kaolinite/halloysite and traces of gibbsite (as was indicated by the IR spectroscopy). The occurrence indicates an acidic environment probably caused by oxidation of sulfides.

The determination of the structural formula, to further characterize the Zn-rich smectite, was difficult because of the multi-clay mineral assembly. However, different SEM-EDX (energy dispersive X-ray) approaches as well as transmission electron microscopy (TEM)-EDX analysis helped to characterize the smectite as Al-rich sauconite with some exchangeable K^+.

KEYWORDS: sauconite, montmorillonite, Silver Coin Mine, Zn-rich smectite.

Montmorillonite is the most abundant dioctahedral smectite. Because of the varying portions of tetrahedral charge, most of the montmorillonites are in fact mixtures of the end members montmorillonite (octahedral charge only) and beidellites (tetrahedral charge only, e.g. Jasmund & Lagaly, 1993). These smectites dominate in bentonites which are mined for various purposes. Other common smectites are nontronite (Fe) and saponite (Mg) both of which occur widely in mafic volcanic rocks such as basalts or diabases (Grim & Güven, 1978; Kaufhold *et al.,* 2012a). Smectites, however, also form in the presence of other di- or trivalent cations such as Cr (volkonskoite) and Zn (sauconite). Sauconite from the type locality (Ueberroth Mine, Saucon Valley, near Friedensville, Pennsylvania, USA) was included in Dana's *System of Mineralogy* in 1968 (p. 409) and in a summary of minerals from Pennsylvania (Genth, 1875). A first comprehensive study of the composition of sauconite from different localities was provided by Ross (1946) who considered the structural formulae in particular. Later, the same materials were investigated for their thermal properties (Faust, 1951). Based on cation exchange experiments, the latter author reported ~0.2 mass% K_2O of the samples as being non-exchangeable (either strongly bound or in mixed-layer minerals). Hemimorphite and halloysite were also reported. A comprehensive study of the chemical differences between different sauconites such as that provided by Ross (1946; Table 1) has not been

* E-mail: s.kaufhold@bgr.de
DOI: 10.1180/claymin.2015.050.4.01

TABLE 1. Comparison of chemical compositions of sauconite. The chemical composition of the sauconite range (column six below) may be affected by traces of halloysite (Faust, 1951).

[mass %]	Sauconite, Friedensville (*Handbook of Mineralogy*, Ross, 1946)	Sauconite, Coon Hollow mine (*Handbook of Mineralogy*, Ross, 1946)	Sauconite webminerals.com (calculated composition of 'ideal' sauconite)	Sauconite, Peru (Mondillo *et al*., 2014)	Sauconite, range Faust (1951), Ross (1946)
SiO_2	34.5	33.4	31.1	34–40	33–39
TiO_2	0.2	0.2			0–0.3
Al_2O_3	17.0	7.5	8.8	3.6–9.1	6–17
Fe_2O_3	6.2	1.7		0.3–3.1	0–6
MnO					0–0.1
MgO	1.1	0.8		0.3–0.6	0.7–1.6
CaO		1.9		1.5	0.6–1.9
Na_2O		0.2	1.6	0.5	0–0.4
K_2O	0.5	0.3		0.7	0–0.5
LOI	17.4	16.9	15.5		15–19
ZnO	23.1	36.7	42.1	38–45	22–40

published since then. In fact most of the data published about the chemical compositions of sauconites (e.g. in the *Handbook of Mineralogy* (Anthony *et al*., 2015); http://webmineral.com, etc.) seems to be based on the work of Ross (1946). In their collection of clay-mineral data, Jasmund & Lagaly (1993) distinguished Al-rich sauconite ($^{VI}Al \approx 1$) from Al-poor sauconite ($^{VI}Al \approx 0.2$), in agreement with Ross (1946).

Higashi *et al.* (2002) and Vogels *et al.* (2005a,b) synthesized sauconite and prepared the hectorite analogue of Zn-rich smectites, i.e. they incorporated Li in the octahedral sheet of Zn-rich smectites. After acid treatment, Mitra & Sindhu (1971) investigated the autotransformation of sauconite sample 4 of Ross (1946). In several studies (e.g. that by Boni *et al.,* 2009) the occurrence of sauconite, often referred to as "non-sulphide Zn-ore", is mentioned but the structural formula has rarely been determined. Boni *et al.* (2009) published a SEM image of sauconite from a Peruvian deposit showing the rose-like aggregates typical of smectites. The range of the chemical composition of this sauconite (SiO_2: 30–36 mass%, ZnO: 34–44 mass %, Al_2O_3: 4–7 mass%, FeO, CaO, and MgO < 2%) is in accordance with the data published by Ross in 1946. Sauconite may be important as ore in non-sulfide zinc deposits (Miller *et al.*, 1941; Borg *et al.,* 2003; Hitzmann *et al.,* 2003; Rollinson *et al.,* 2011).

In the Silver Coin Mine (SWT sec. 1 and SET sec. 2, T35N, R41E, Valmy, Iron Point district, Humboldt County, Nevada, USA; Mills *et al.,* 2011), five new minerals have been discovered so far (www.mindat.org): fluorowardite (hydrous Na-Al-F-phosphate), iangreyite (hydrous Ca-Al-F-phosphate), krásnoite (hydrous Ca-Al-Si-F-phosphate), meurigite-Na (hydrous Na-Fe-phosphate), and zinclipscombite (Zn-Fe-phosphate) (Chukanov *et al.,* 2006; Kampf *et al.,* 2009, 2012; Mills *et al.,* 2011, 2012). Basic information about the geological setting of the mine was published by Vanderburg (1988) and Kampf *et al.* (2012). In the Silver Coin Mine Pb-Zn-Ag-veins occur within thin-bedded quartzite, argillite and phosphatic argillite of late Palaeozoic age (Vanderburg, 1988). The mine was active from 1918 to 1924 in shallow shafts, open cuts, and surface trenches. According to Mills *et al.* (2011) "veins consisting of quartz, barite, pyrite, argentiferous galena and sphalerite filled a fault zone and associated fractures". In addition to the sulfides, minerals typical of oxidation zones as well as secondary phosphates (previously leached from the phosphatic host rocks) were found. The combination of hydrothermal mineralization and phosphatic rocks obviously led to the formation of a variety of minerals. More than 100 minerals have been found in the Silver Coin Mine (www.mindat.org). The occurrence of Zn-rich smectites has not been reported until now.

The aim of the present study was to characterize those clay minerals found in the unique Silver Coin mine.

MATERIALS AND METHODS

A clay sample was collected in the Silver Coin Mine during 2011. The sample was collected from a heap of

https://doi.org/10.1180/claymin.2015.050.4.01 Published online by Cambridge University Press

gel-like mud with material showing white to greenish mm-sized veins. A 100 g sample showing green and white clayey veins was used for analysis (Fig. 1).

The use of SEM coupled with EDX revealed that there is no difference between the white and the light green clay. The amount of the clayey material was too small for a comprehensive analysis but SEM investigations suggested that particle-size separation would help to produce a sample with sufficiently high concentration of clay minerals. The sample was crushed with a jaw crusher down to <1 mm, mixed with 1 L of deionized water, allowed to swell for 1 week and then placed in an ultrasonic bath for 2 h. The suspension was then transferred to a 5 L beaker and 4 L of water was added. After 48 h of stirring, the suspension was allowed to settle. After a further 4 days, a well dispersed fraction was observed in the uppermost (20 cm) part of the beaker. This fraction was collected twice and designated as a '<0.5 μm' fraction because, considering temperature, time of sedimentation, and depth of collecting of the suspension, this fraction should be ≪1 μm and is expected to represent the smectite fraction of the sample. After collecting the '<0.5 μm' fraction, the rest of the suspension was split with a 20 μm sieve into <20 μm and >20 μm fractions. The suspensions were centrifuged and dried at 60°C. The three samples were labelled as ZnS-1, ZnS-2 and ZnS-3 ('<0.5 μm fraction' = ZnS-1, <20 μm fraction = ZnS-2 and >20 μm fraction = ZnS-3).

X-ray diffraction patterns of randomly oriented samples were recorded using a PANalytical X'Pert PRO MPD θ-θ diffractometer (Cu*K*α radiation generated at 40 kV and 30 mA), equipped with a variable divergence slit (20 mm irradiated length), primary and secondary Soller slits, a Scientific X´Celerator detector (active length = 0.59°), and a sample changer (sample diameter = 28 mm). The samples were investigated from 2 to 85°2θ with a step size of 0.0167°2θ and a measuring time of 10 s per step. For specimen preparation the top-loading technique was used.

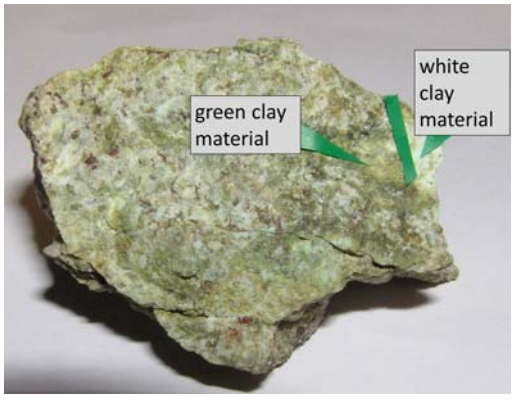

FIG. 1. Photograph of the investigated sample (image width = 8 cm) with white and green clay coatings.

Small proportions of the '<0.5 μm' fraction (Na-, Ba- and Cu_{trien}-intercalated – Kaufhold *et al.,* 2011b) were measured with 10 mm irradiated length and point detector (proportional counter) to access data suitable for a structural characterization by the Rietveld method using the smectite structural model described by Ufer *et al.* (2008). Side loading was used to minimize the effect of preferred orientation. Rietveld refinement was difficult because of the low degree of structural order observed despite Cu_{trien} intercalation.

Sample ZnS-1 was also investigated as a 'texture slide' (natural cation population with preferred orientation). The slide was prepared by suction of a suspension through a porous ceramic plate. The XRD pattern was recorded using Co radiation.

The chemical composition of the powdered samples was determined using a PANalytical Axios and a PW2400 spectrometer. Samples were prepared by mixing with a flux material (Lithiummetaborate Spectroflux, Flux No. 100A, Alfa Aesar) and melting into glass beads. The beads were analysed by wavelength dispersive X-ray fluorescence spectrometry (WD-XRF). To determine loss on ignition (LOI), 1000 mg of sample material was heated to 1030°C for 10 min.

The cation exchange capacity (CEC) was determined according to Meier & Kahr (1999) using the Cu_{trien} method which was discussed by Kaufhold & Dohrmann (2003). The accuracy of this method was discussed by Dohrmann *et al.* (2012).

To measure mid-infrared (MIR) spectra, the KBr pellet technique (1 mg sample/200 mg KBr) was applied. Spectra were collected using a Thermo Nicolet Nexus FTIR spectrometer (MIR beam splitter: KBr, detector DTGS TEC). The resolution was adjusted to 2 cm^{-1}.

Simultaneous thermal analysis (STA) was performed using a Netzsch 449 F3 Jupiter thermobalance equipped with a differential scanning calorimetry/thermogravimetry (DSC/TG) sample holder linked to a Netzsch QMS 403 C Aeolus mass spectrometer (MS). 100 mg of powdered material previously equilibrated at 53% relative humidity (RH) was heated from 25 to 1100°C at a heating rate of 10°C/min.

For investigation by SEM, an FEI Quanta 600 F instrument operated in low-vacuum mode (0.6 mbar) was

https://doi.org/10.1180/claymin.2015.050.4.01 Published online by Cambridge University Press

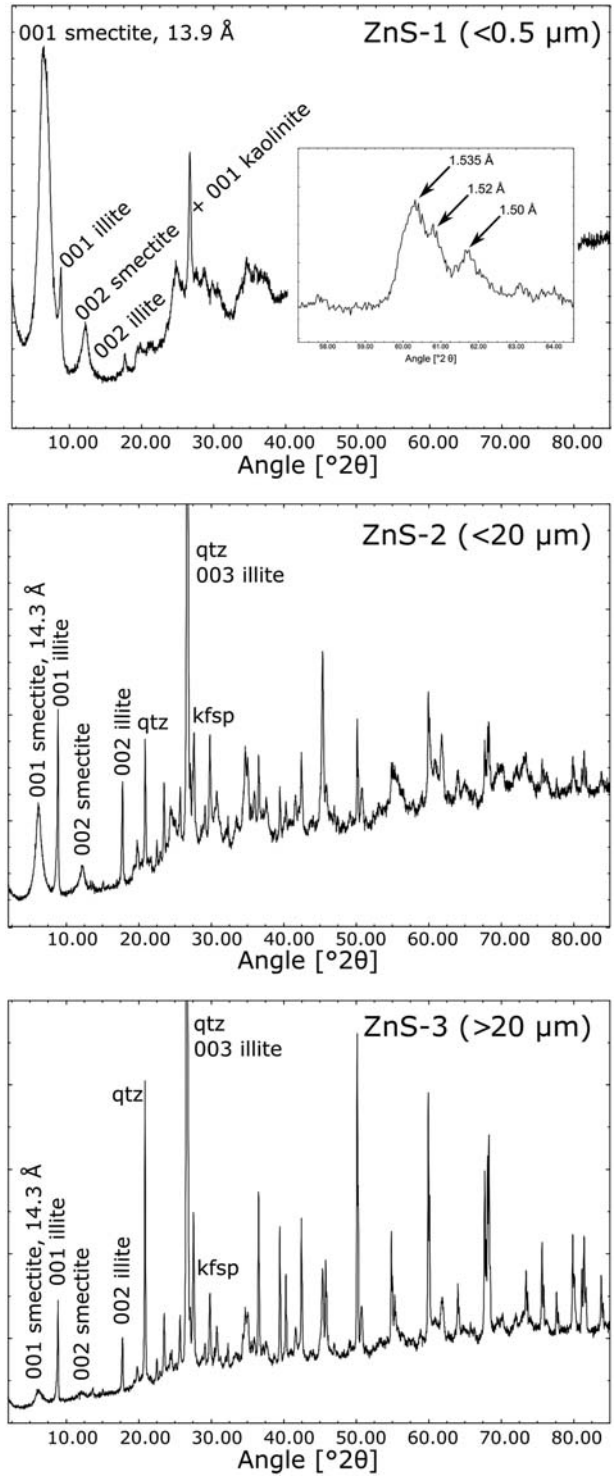

FIG. 2. Powder XRD patterns of the three fractions ZnS-1, ZnS-2 and ZnS-3. The inset shows a close-up of the 060 reflection.

https://doi.org/10.1180/claymin.2015.050.4.01 Published online by Cambridge University Press

used. Sputtering of the samples with gold or carbon was not necessary, therefore. The microscope is equipped with the EDX-system Genesis 4000 from EDAX.

For TEM analyses, the <0.5 µm fraction was dispersed ultrasonically followed by dropping the suspension on a TEM copper grid stretched C-film. The analyses were run on an analytical Jeol JEM 1210 at 120 kV. Energy dispersive X-ray spectra (TEM-EDX) were recorded with a count time of 10 s to reduce K^+ migration using an Oxford instruments Pentafel Link/Model 6635 (30 mm²) SiLi detector. In general the Si^{4+} content was overestimated and Na^+ values contain the largest error due to the analytical difficulties in detecting the Na^+ peak. For generating and interpreting the EDX data, the Oxford Instruments *INCA* software package was used.

RESULTS AND DISCUSSION

XRD

The XRD powder pattern of sample ZnS-1 (<0.5 µm) showed the dominance of a 14 Å phase and minor amounts of a 10 Å phase. The coarser fractions also contain quartz and feldspar (Fig. 2). For a more detailed investigation of both peaks and of the 7 Å peak which might be attributed to the d_{002} of the 14 Å phase or to a kaolin mineral, oriented slides were prepared (Fig. 3). After EG solvation a d_{001} diffraction maximum at ~17 Å was observed, the second-order maximum was located at 8.4 Å and the d_{005} maximum at 3.35 Å. This integral series is indicative of well-ordered stacking sequences of smectite with insignificant interstratification. For a more detailed analysis of possible interstratification, a greater number of basal peaks must be considered. The intensities of these additional maxima decrease with increasing *d* spacing and hence were not considered further. The positions of the first three peaks alone do allow us to establish interstratification to a limited extent.

The peak at 10 Å neither changed its position upon K-saturation nor upon EG solvation and hence this peak was assigned to illite. A broad maximum at ~7.2–7.3 Å was observed after air-drying and EG solvation. In the EG pattern a weak peak at 3.58 Å was detected. These peaks were better resolved after treatment of the oriented specimen with K ions which shifted the basal reflections of the smectite to larger angles. According to XRD data, the 7.2–7.3 peak was attributed to kaolinite/halloysite.

The position of the diagnostic d_{060} reflection is at 1.535 Å (Fig. 2, inset). This peak, however, shows a pronounced shoulder towards lower *d* spacings (1.52 Å) which indicates the presence of some

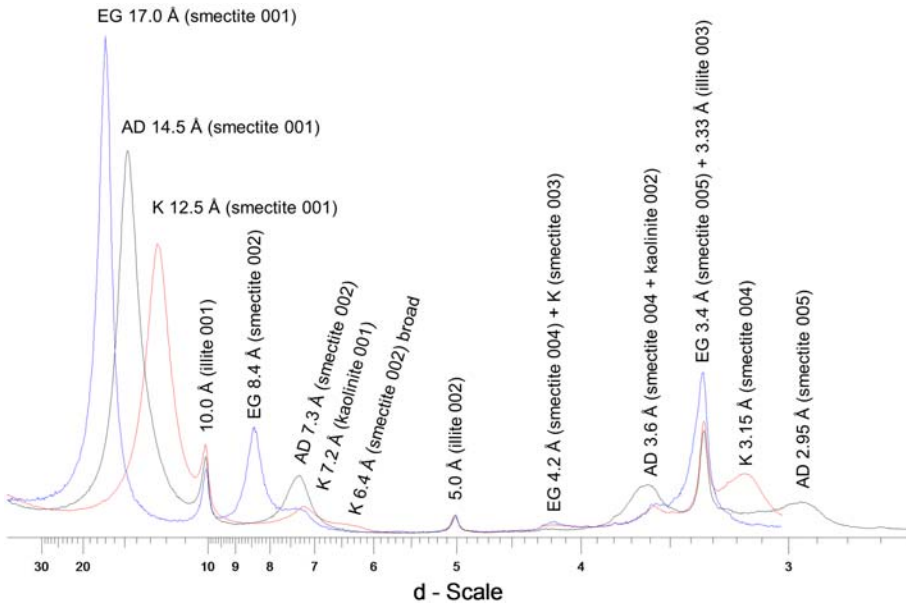

FIG. 3. XRD oriented slides (AD: air-dried, K: K-saturated, EG: EG-solvated) of ZnS-1 (<0.5 µm).

https://doi.org/10.1180/claymin.2015.050.4.01 Published online by Cambridge University Press

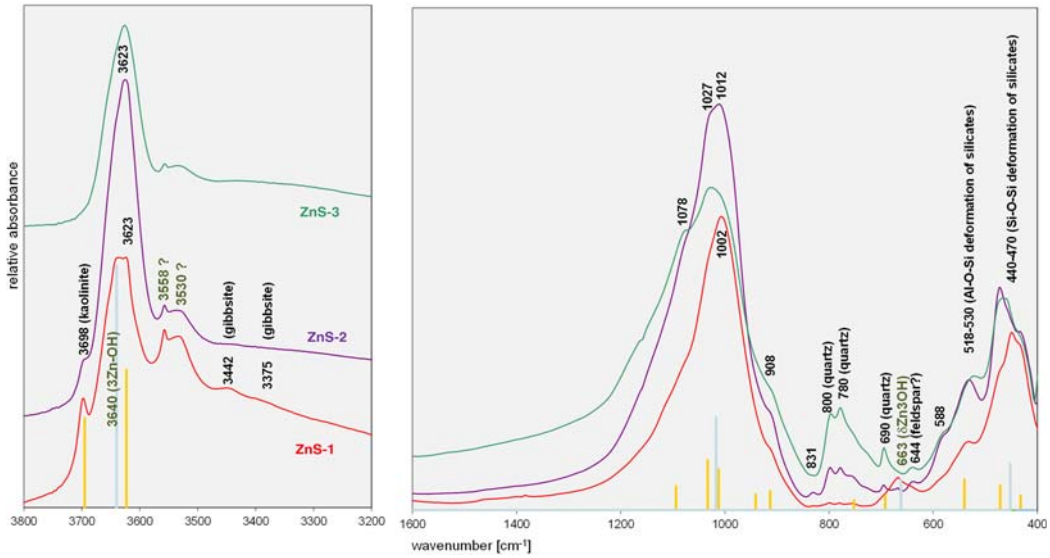

FIG. 4. IR spectra of the three fractions.

dioctahedral layers or at least domains. The peak at 1.50 Å was assigned to illite but kaolin may also contribute to it (in spite of the small amount of this mineral present). Rietveld refinement indicated the dominance of smectite (~50%) and illite (~40%) but the fits were of low quality because the structural

TABLE 2. Chemical composition of the three fractions compared to the range of sauconite compositions (major elements).

[mass %]	Sauconite, range Faust (1951), Ross (1946)	ZnS-1 <0.5 μm	ZnS-2 <20 μm	ZnS-3 >20 μm
SiO_2	33–39	38.0	52.9	70.1
TiO_2	0–0.3	0.3	0.6	0.5
Al_2O_3	6–17	11.5	16.6	11.2
Fe_2O_3	0–6	7.6	5.2	4.5
MnO	0–0.1	0.0	0.0	0.0
MgO	0.7–1.6	3.0	1.5	0.7
CaO	0.6–1.9	0.7	0.3	0.2
Na_2O	0–0.4	0.0	<0.01	<0.01
K_2O	0–0.5	3.6	7.0	5.5
P_2O_5		0.2	0.2	0.2
SO_3		0.1	0.0	<0.01
(Cl)		0.0	<0.002	0.0
(F)		<0.05	<0.05	<0.05
ZnO	22–40	21.0	7.7	2.8
LOI	15–19	14.0	6.1	3.0
Cu		0.90	0.40	0.20
Pb				
Ni				
SUM	100.0	100.8	98.6	98.9

https://doi.org/10.1180/claymin.2015.050.4.01 Published online by Cambridge University Press

TABLE 3. Chemical composition of the three fractions of the sample (trace elements).

[mg/kg]	ZnS-1 <0.5 µm	ZnS-2 <20 µm	ZnS-3 >20 µm	[mg/kg]	ZnS-1 <0.5 µm	ZnS-2 <20 µm	ZnS-3 >20 µm
(As)	892	579	476	Pb	6360	8437	4853
Ba	428	921	911	Rb	372	367	230
Bi		5	<3	Sb	1240	975	792
Ce		42	46	Sc		10	10
Co	548	196	69	Sm		20	17
Cr	72	193	122	Sn		<14	<13
Cs	228	37	28	Sr	164	64	48
Cu	8968	4518	2369	Ta		<7	<5
Ga	68	39	22	Th	44	17	10
Hf		<9	<7	U		10	8
La		39	24	V	396	389	217
Mo		<3	<3	W		21	21
Nb	24	12	10	Y	36	27	28
Nd		<14	<13	Zr	232	76	180
Ni	1700	689	260				

disorder could not be described properly. The clay mineral assemblage sauconite, illite and kaolinite was reported by Mondillo *et al.* (2014).

XRF – chemical composition

The chemical composition of the '<0.5 µm fraction' (dominated by smectite according to XRD results) corresponds to the values given for sauconites (Ross, 1946; Faust, 1951; Table 2) except for the K_2O value. The sample investigated in the present study showed much larger K_2O values than the typical sauconites, which may be explained by the illite content of ZnS-1. Indeed, ZnS-1 contains 3.6 mass% K_2O which corresponds to ~50% illite assuming a K_2O content of 7–7.5% for pure illite. Rietveld refinement yielded 40% illite. Some of the K may be in the smectite, therefore.

The sum of the major elements did not reach 100 mass% because of the presence of >1 mass% Cu and Pb in samples ZnS-2 and ZnS-3 (Table 3). The distributions of Cu and Pb are further investigated by SEM-EDX.

IR spectroscopy

ZnS-1 showed a well resolved band at 663 cm^{-1} which can be assigned to Zn_3OH deformation

TABLE 4. CEC and exchangeable cations determined by inductively coupled plasma-mass spectrometry of the three fractions.

Sample	mass [g]	Na^+ $cmol_c/kg$	K^+ $cmol_c/kg$	Mg^{2+} $cmol_c/kg$	Ca^{2+} $cmol_c/kg$	sum $cmol_c/kg$	CEC $cmol_c/kg$
ZnS-1	0.080	11.3	14.8	20.7	20.3	67.0	45.3
ZnS-1	0.120	12.7	13.7	20.2	20.3	66.9	45.4
ZnS-2	0.080	0.0	1.2	8.5	7.4	17.0	16.0
ZnS-2	0.120	0.0	0.9	8.5	7.4	16.8	15.4
ZnS-3	0.080	0.0	0.5	2.3	2.3	5.2	3.8
ZnS-3	0.121	0.0	0.4	2.3	2.2	4.9	4.7

https://doi.org/10.1180/claymin.2015.050.4.01 Published online by Cambridge University Press

(Yokoyama *et al.*, 2006; Petit *et al.,* 2008). According to the same authors the 3640 cm^{-1} band can be assigned to the Zn_3OH stretching vibration. The band at 3698 cm^{-1} confirms the presence of a kaolin mineral which was indicated by XRD. The detection limit of kaolinite in the IR is comparably low (≤0.5 mass%; Madejova *et al.,* 2002; Kaufhold *et al.,* 2012b) even when smectites are dominant. The presence of traces of gibbsite was also indicated by IR. The assignment of the remaining OH-stretching bands was more difficult. The band at 3623 cm^{-1} could be explained by AlAlOH mostly from the kaolinite. Dioctahedral illite might also contribute to this band. The bands at 3558 and 3530 cm^{-1} might correspond to combinations of Fe-, Mg- and Zn-OH. The spectra of the two sauconites published by van der Marel & Beutelspacher (1976) and of that by Higashi *et al*. (2002) do not show these bands. Tiller & Pickering (1974) published IR spectra but only up to 1700 cm^{-1}. Hence no references for these bands were found. The Mg and Fe contents of sample ZnS-1 are larger than those of most of the published sauconites which may explain the two additional bands. Based on the data provided by Madejova *et al.* (1994) the 3558 cm^{-1} vibration could result from octahedral Fe and/or Mg. This band is typically observed in Fe-rich TOT minerals (not in Fe hydroxides). The broader band at 3530 cm^{-1} might correspond to FeFeOH or to a stretching mode with a slightly lighter and a slightly heavier atom (e.g. MgZnOH). This band could not be assigned unambiguously, therefore. In any case, the IR spectra showed the presence of a Zn-rich smectite.

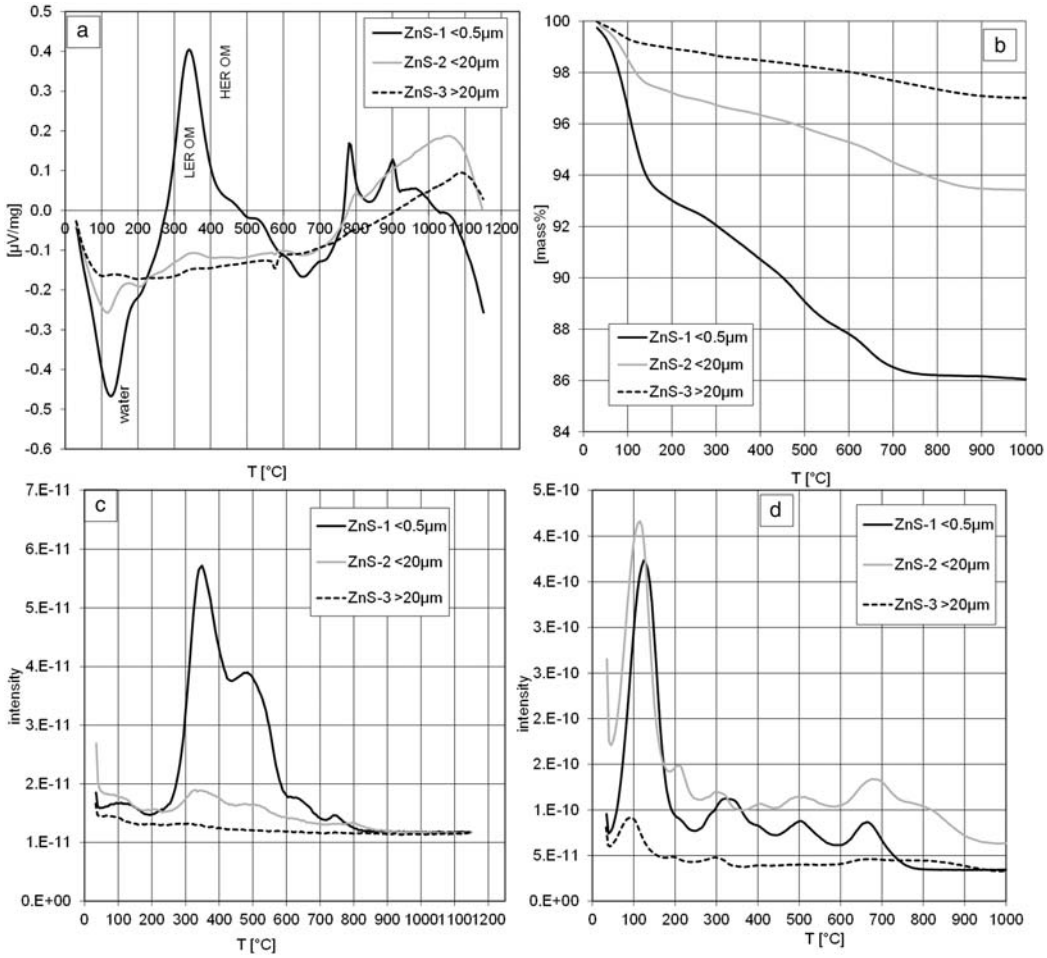

FIG. 5. DTA-MS analysis of the three fractions: (a) DSC, (b) TG, (c) MS-CO_2 and (d) MS-H_2O.

https://doi.org/10.1180/claymin.2015.050.4.01 Published online by Cambridge University Press

CEC

The CEC of sample ZnS-1 was 45 $cmol_c$/kg which, assuming a moderate layer-charge density and variable charge, corresponds to ~50 mass% smectite (Kaufhold *et al.,* 2002; Kaufhold & Dohrmann, 2003). The CEC data indicate the presence of some swelling K-smectite because ~14 $cmol_c$/kg of exchangeable K^+ was found. In addition to the K^+, the interlayer of the ZnS-1 smectite contains ~20 $cmol_c$/kg each of Ca^{2+} and Mg^{2+} and 12 $cmol_c$/kg of Na^+. The sum of exchangeable cations is larger than the CEC, indicating the presence of soluble phases. Considering the CEC and assuming similar layer-charge densities of the smectites in the '<0.5 μm' and the <20 μm size fractions we conclude that ZnS-2 contains 1/3 of the amount of smectites (compared to ZnS-1). The values of exchangeable Ca^{2+} and Mg^{2+} of ZnS-2 confirmed this ratio. The amount of exchangeable Na^+ and K^+ in ZnS-2 was ≪1/3 of ZnS-1, however, suggesting that ZnS-1 contains some soluble Na/K phases. The smectites of samples ZnS-1 and ZnS-2 contain exchangeable K^+ but no exchangeable Na^+. Therefore, one might speculate that ~3 $cmol_c$/kg of K^+ of sample ZnS-1 was from exchange sites (value estimated on the basis of the molar ratios and CEC). The sum of $Na^+ + K^+$ measured for sample ZnS-1 accounts for 26 $cmol_c$/kg and the sum of cations exceeds the CEC by ~22 $cmol_c$/kg. This indicates that 3 $cmol_c$/kg K^+ would be from the smectite exchange sites resulting in 23 $cmol_c$/kg of $Na^+ + K^+$ from soluble phases.

Thermal analysis

The first DSC signal at ~120°C could be assigned to dehydration of smectites. Because of the larger smectite content in ZnS-1 compared to the others, this signal has a greater intensity (Figure 5a). The MS curve of water (Fig. 5d) indicated that the dehydration consists of two reactions. The most pronounced DSC signal at 330°C resulted from the oxidation of organic matter which, according to the classification of Friedrich *et al.* (1996) is dominated by easily oxidized organic matter (low exothermic reaction – LER, dominates over high exothermic reaction – HER). As a result two distinct peaks of the MS-CO_2 curves were observed, the first at 330°C and the second at ~500°C. The MS-H_2O curves contained three resolved peaks between 300 and 500°C indicating a three-step oxidation of the organic matter or an additional effect of gibbsite which was detected by IR. The endothermal DSC peak at ~650°C was assigned to the dehydroxylation of the smectite because a corresponding peak was found in the MS-H_2O curve. The sharp exothermal DSC peaks at ~800 and 900°C were attributed to recrystallization. The deyhdroxylation temperature of kaolinite and illite would be ~500°C. The sample with the most abundant illite (ZnS-3), however, showed the smallest MS-H_2O peak which indicated that this peak could be assigned to water from oxidation of organic matter.

Electron microscopy

Smectites are distinguished according to their chemical composition which is used to calculate a structural formula. The chemical composition of the '<0.5 μm fraction' could not be used for the calculation of a structural formula because this fraction was not pure and the illite content could not be determined with sufficient accuracy for correction. Investigation by SEM of the uncrushed sample (Fig. 6) revealed different morphologies of the clay-particle aggregates which could not always be assigned to a specific mineral. As an example, rounded aggregates are present which showed one protuberance each (Fig. 6, left). In addition, at the walls of cavities which contained large crystals, tightly arranged smectites were observed in a 10 μm-thick layer. The matrix also contained some smectite.

To separate the different clay minerals, the sample was saturated with $BaCl_2$, dialyzed and slow sedimentation applied. The Ba exchange provided information about the layer charge from EDX data because the Ba measured with EDX can only be in exchangeable sites within the smectite interlayer.

A 100 μm-thick fragment of the Ba-saturated ZnS-1 sample was investigated by electron microscopy (Fig. 7, left). Laminated/textured clay mineral fragments were also found as small, bright particles (Fig. 7, right). The diameters of these small, bright particles ranged from 0.1 to 0.5 μm and EDX analysis revealed Pb, Cu and C. Because of their small diameter they could not be analysed by EDX without interference from Al and Si in adjacent clay minerals. Therefore, the formula was not calculated for these minerals. No EDX analysis of the clay minerals could be recorded in which Pb and Cu were absent (<0.2 mass%). The small Pb/Cu content (below the EDX detection limit) in areas where bright particles were absent, indicated their absence from the clay minerals. Ten EDX analyses performed at the top of the sediment layer (smectites were thought to be concentrated at the top due to their generally smaller particle size) were used to calculate

https://doi.org/10.1180/claymin.2015.050.4.01 Published online by Cambridge University Press

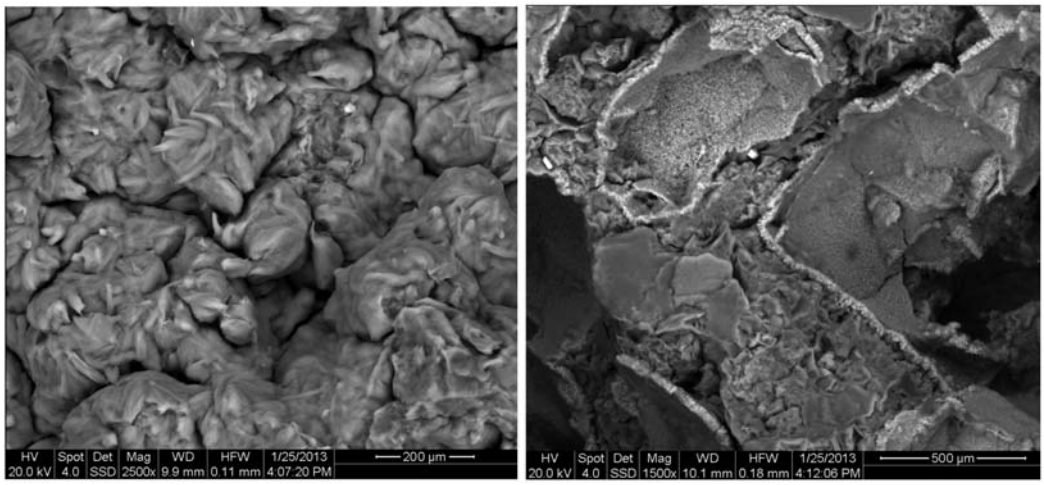

FIG. 6. SEM images of a freshly broken surface of the studied sample.

the structural formula. Surprisingly, despite the fact that Ba was used to saturate permanent charges, K and Ca were still present. These cations are considered to be part of the adsorbed cation pool. They are obviously non-exchangeable, however. Kaufhold *et al.* (2011a) showed the presence of such non-exchangeable, non-structural cations particularly in high-charged dioctahedral smectites. They could also exist in Zn-rich smectites. Alternatively, the cation exchange for Ba might have been incomplete. The structural formula, in turn, was calculated considering the exchangeable interlayer cations as well as the non-exchangeable, non-structural cations. Hence, the sum of octahedral cations and the tetrahedral charge were variable. This calculation, however, led to a structural formula with Ba as the exchangeable cation. For the calculation of the final structural formula, the Ba was replaced by Ca and Mg (according to CEC measurements) based on the assumption that the Cu_{trien} (CEC experiment) exchanged the same amount of cations as the Ba. The interlayer was still dominated by K though most of the K present after the CEC experiment was thought to result from soluble phases and hence was disregarded. The EDX analysis, therefore, indicated the presence of

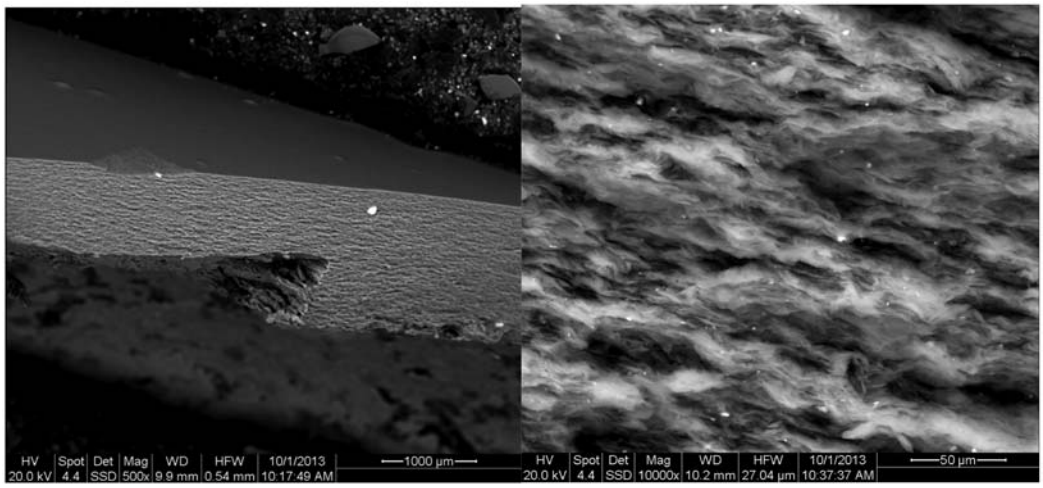

FIG. 7. SEM images of the Ba-saturated ZnS-1 sample.

https://doi.org/10.1180/claymin.2015.050.4.01 Published online by Cambridge University Press

TABLE 5. Structural formula of the Silver Coin Mine Zn-rich smectite compared with published structural formulae of Zn-rich smectites (assumption: all Fe = ferric Fe, error discussed by Kaufhold *et al.*, 2011a).

		(Zn	Mg	Al	Fe)	(Al	Si)	O_{10} $(OH)_2$ X^-		
	1	1.48	0.14	0.74	0.4 $_{2.8}$	0.99	3.01 $_{4.0}$	0.33	Friedensville	Ross (1946)
	2	2.4	0.18	0.22	0.17 $_{3.0}$	0.53	3.47 $_{4.0}$	0.35	New Discovery Mine Leadville	Ross (1946)
	3	1.85	0.14	0.79	0.02 $_{2.8}$	0.7	3.3 $_{4.0}$	0.51	Yankee Doodle Mine, Leadville	Ross (1946)
	4	2.64	0.11	0.12	0.13 $_{3.0}$	0.73	3.27 $_{4.0}$	0.88	Coon Hollow Mine, brown	Ross (1946)
	5	2.89	0.1	0.04	0.02 $_{3.1}$	0.65	3.35 $_{4.0}$	0.83	Coon Hollow Mine, white	Ross (1946)
	6	1.54	0.15	0.78	0.23 $_{2.7}$	0.61	3.39 $_{4.0}$	0.38	Liberty Mine, Meekers Grove	Ross (1946)
	7	1.23	0.41	0.73	0.43 $_{2.8}$	0.8	3.2 $_{4.0}$	0.33	Plattesville District	Ross (1946)
	8	1.95	0.12	0.17	0.58 $_{2.8}$	0.61	3.39 $_{4.0}$	0.33	Friedensville, pale yellow	Ross (1946)
	9	2.46	0.1	0.38	0 $_{2.9}$	0.61	3.39 $_{4.0}$	0.8	Lower Waterloo Mine, Leadville	Ross (1946)
	10	2.32	0.1	0.55	$_{3.0}$	0.62	3.38 $_{4.0}$	0.68	Lower Waterloo Mine, Leadville	Ross (1946)
	11	2.8-x	x	0.2-y	y $_{2.8}$	0.6	3.4 $_{4.0}$	0.4	'sauconite'	Jasmund & Lagaly (1993)
	12	1.8-x	x	1-y	y $_{2.8}$	0.8	3.3 $_{4.1}$	0.2	'Al rich sauconite'	Jasmund & Lagaly (1993)
	13	2.6	0.2	0.1	0.1 $_{3.0}$	0.6	3.4 $_{4.0}$	0.4	'average sauconite'	Köster (1982)
	14	1.6	0.2	0.8	0.2 $_{2.8}$	0.8	3.2 $_{4.0}$	0.2	'average Al-sauconite'	Köster (1982)
x1	(K, Ca, Mg)	(Zn	Mg	Al	Fe)	(Al	Si)	O_{10} $(OH)_2$ X^-	Silver Coin	present study
	0.2 0.15 0.05	1.1	0.3	0.7	0.4	0.5	3.5	0.4	Silver Coin	SEM_{Ba} + CEC
x2	(1/2 Cu_{trien})	(Zn	Mg	Al	Fe)	(Al	Si)	O_{10} $(OH)_2$ X^-	Silver Coin	present study
	0.4	1.1	0.3	*1.2*	0.4	0.6	3.4	0.4	Silver Coin	SEM Cu_{trien}
x3	Na	(Zn	Mg	Al	Fe)	(Al	Si)	O_{10} $(OH)_2$ X^-	Silver Coin	present study
	0.4	2.3	0.3	0.3	0.0	0.4	3.6	0.4	Silver Coin	TEM

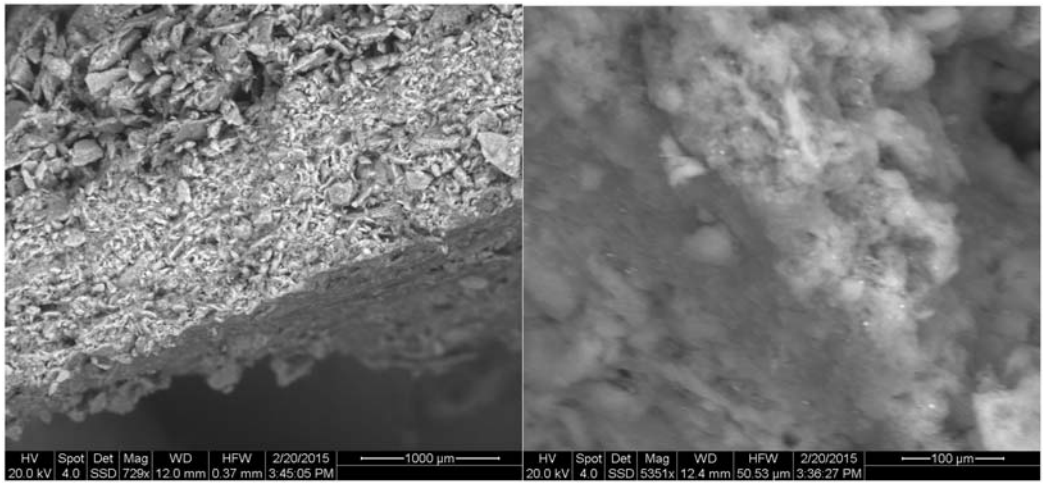

FIG. 8. SEM images of the Cu_{trien}-exchanged ZnS-1 sample (sedimented slowly).

more interlayer K than discussed in the section on CEC above. The structural formula derived from SEM-EDX of the Ba-saturated sample, taking into account the CEC data (Ba replaced by the results of CEC measurements), is given in Table 5 (x1). To exclude artefacts caused by an incomplete Ba exchange, ZnS-1 was also saturated with Cu_{trien} and again a sediment was produced for SEM-EDX analysis in which the smectites were assumed to be concentrated at the top of the sediment (Fig. 8). Again ten EDX analyses of the uppermost section were recorded and fine-grained dense minerals (white spots) were noted to contain Cu, Pb and C (Fig. 8). The SEM-EDX investigations of the Cu_{trien} sample confirmed results obtained on the Ba sample (Table 5, x2). The layer-charge density of formula x2 was calculated on the basis of the Cu value (care was taken to investigate areas without white spots) and of the Ca and K values, neither of which was exchanged for the Cu-trien (non-exchangeable cations were reported previously, e.g. by Kaufhold *et al.*, 2011a).

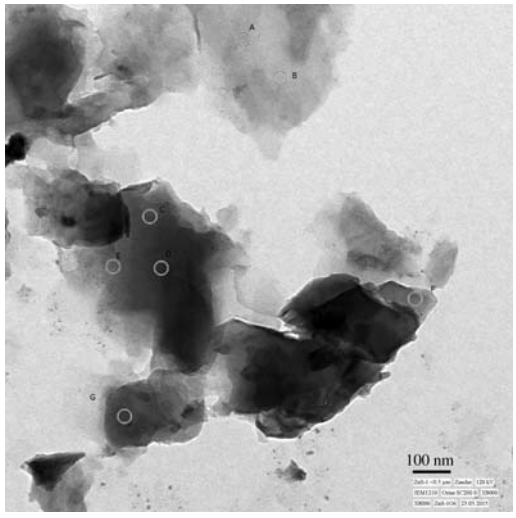

FIG. 9. Representative TEM image of EDX analysis spots.

Despite the presence of the small Cu/Pb/C minerals a comparable formula was obtained with a much larger Al content (which may result from amorphous Al-phase by-products of acid alteration). The resulting formula (x2) is not rational because the octahedral layer would have more positive charge than negative charge in the tetrahedral layer.

As explained above, the structural formula derived from SEM-EDX investigations (x1, x2 in Table 5) could be affected by the presence of amorphous Al/Fe-oxyhydroxides. Consequently, additional TEM-EDX analyses were performed. A representative TEM image is given in Fig. 9. The structural formula calculated on the basis of the marked EDX measuring spots (Fig. 9) is given in Table 5 (x3). In contrast to SEM-EDX the smectite has much smaller Fe and higher Zn contents. Fe was only detected at measurement points where dark needles (possibly goethite) occurred (H in Fig. 9). The Fe content of the smectite may, therefore, be smaller than determined by SEM-EDX. The layer-charge density, however, in addition to octahedral and tetrahedral Al, is similar to the Ba sample. Three

https://doi.org/10.1180/claymin.2015.050.4.01 Published online by Cambridge University Press

independent electron microscope methods have indicated the presence of an Al-containing sauconite. The accuracy of the three structural formula methods was not sufficient to establish similarities with one of the published formulae given in Table 5. The smectite, however, could be identified clearly as sauconite because it falls within the normal range of sauconite compositions.

SUMMARY AND CONCLUSIONS

In the Silver Coin Mine (Humboldt County, Nevada, USA) >100 minerals were found including several Zn-phases; Zn-rich smectites had not been discovered at the mine, however.

In the present study a greenish clayey material collected at the mine was analysed using clay-mineralogical methods. Analyses focused on the fine fraction of the sample which was produced by sedimentation. The sharp and symmetric basal XRD reflections observed after different treatments indicated the presence of smectite. The position of the 060 reflection indicated the dominance of trioctahedral clay minerals physically mixed with some dioctahedral clay minerals. Illite and a dioctahedral mineral of the kaolin group were detected using XRD. Infrared spectroscopy confirmed the presence of kaolinite/halloysite and traces of gibbsite; the presence of very fine grained Pb-Cu-C-rich particles was verified by electron microscopy. The fine fraction contained 3.6 mass% K_2O which theoretically would correspond to ~50 mass% illite; Rietveld refinement yielded 40% illite. SEM-EDX analyses of the Ba-saturated fine fraction showed the presence of non-exchangeable K^+ in the smectite. Using SEM-EDX and TEM-EDX, slightly different structural formulae were obtained. The accuracy of the three structural formula methods was insufficient to establish unambiguously similarities with one of the published formulae. The smectite could be identified clearly as sauconite, however, because it falls within the normal range of sauconite compositions.

REFERENCES

Anthony J.W. Bideaux R.A., Bladh K.W. & Nichols M.C. (editors) *Handbook of Mineralogy.* Mineralogical Society of America, Chantilly, VA, USA. http://www.handbookofmineralogy.org/ (accessed in 2015).

Boni M., Balassone G., Arseneau V. & Schmidt P. (2009) The nonsulfide zinc deposit at Accha (southern Peru). Geological and mineralogical characterization. *Economic Geology*, **104**, 267–289.

Borg G., Kärner K., Buxton M., Armstrong R. & Van Der Merwe S.W. (2003) Geology of the Skorpion supergene zinc deposit, southern Namibia. *Economic Geology*, **98**, 749–771.

Chukanov N.V., Pekov I.V., Möckel S., Zadov A.E. & Dubinchuk V.T. (2006) Zinclipscombite $ZnFe_2^{3+}(PO_4)_2(OH)_2$ – a new mineral. *Proceedings of the Russian Mineralogical Society*, **135**(6), 13–18.

Dohrmann R., Genske D., Karnland O., Kaufhold S., Kiviranta L., Olsson S., Plötze M., Sandén T., Sellin P., Svensson D. & Valter M. (2012) Interlaboratory CEC and exchangeable cation study of bentonite buffer materials: II. Alternative methods. *Clays and Clay Minerals*, **60**, 176–185.

Friedrich A., Grunewald K., Klinnert S. & Bechmann W. (1996) Thermogravimetric and differential thermal analytical investigations on sewage farm soils. *Journal of Thermal Analysis and Calorimetry*, **46**, 1589–1597.

Genth F.A. (1875) *Preliminary Report on the Mineralogy of Pennsylvania*. Pennsylvania Geological Survey, 2nd report, p. 120.

Grim R.E. & Güven N. (1978) *Bentonites – Geology, Mineralogy and Uses.* Developments in Sedimentology, **24**. Elsevier, Amsterdam.

Higashi S., Miki K. & Komarneni S. (2002) Hydrothermal synthesis of Zn-rich smectites. *Clays and Clay Minerals*, **50**, 299–305.

Hitzman M.W., Reynolds N.A., Sangster D.F., Allen C.R. & Carman C.E. (2003) Classification, genesis, and exploration guides for nonsulfide zinc deposits. *Economic Geology*, **98**, 685–714.

Jasmund K. & Lagaly G. (1993) *Tonminerale und Tone*. Steinkopf Verlag, Darmstadt, Germany, 490 pp.

Kampf A.R., Adams P.M., Kolitsch U. & Steele I.M. (2009) Meurigite-Na, a new species, and the relationship between phosphofibrite and meurigite. *American Mineralogist*, **94**, 720–727.

Kampf A.R., Adams P.M. & Housley R.M. (2012) Fluorowardite, IMA 2012-016. CNMNC Newsletter No. 13, June 2012, page 816; *Mineralogical Magazine*, **76**, 807–817.

Kärner K. (2006) *The Metallogenesis of the Skorpion Non-Sulphide Zinc Deposit, Namibia*. Dissertation, Martin-Luther-Universität Halle-Wittenberg, 252 pp.

Kaufhold S. & Dohrmann R. (2003) Beyond the methylene blue method: determination of the smectite content using the Cu-trien method. *Zeitschrift für Angewandte Geologie*, **2**, 13–18.

Kaufhold S., Dohrmann R., Ufer K. & Meyer F.M. (2002) Comparison of methods for the quantification of montmorillonite in bentonites. *Applied Clay Science*, **22**, 145–151.

Kaufhold S., Dohrmann R. & Stucki J. (2011a) Layer charge density of montmorillonite – closing the gap between structural formula method and alkyl ammonium method. *Clays and Clay Minerals*, **59**, 200–211.

https://doi.org/10.1180/claymin.2015.050.4.01 Published online by Cambridge University Press

Kaufhold S., Dohrmann R., Ufer K., Kleeberg R. & Stanjek H. (2011b) Cu trien exchange to improve the analytical understanding of smectites. *Clay Minerals*, **46**, 411–420.

Kaufhold S., Dill H.G. & Dohrmann R. (2012a) Clay mineralogy and rock strength of a mid-German diabase – implications for improved quality control. *Clay Minerals*, **47**, 419–428.

Kaufhold S., Hein M., Dohrmann R. & Ufer K. (2012b) Quantification of the mineralogical composition of clays using FTIR spectroscopy. *Journal of Vibrational Spectroscopy*, **59**, 29–39.

Köster H.M. (1982) The crystal structure of 2:1 layer silicates. pp. 41–71 in: *Proceedings of the International Clay Conference*, Bologna, Pavia, 1981 (H. Van Olphen and F. Veniale, editors). Elsevier, Amsterdam.

Madejová J., Komadel P. & Čičel B. (1994) Infrared study of octahedral site populations in smectites. *Clay Minerals*, **29**, 319–326.

Madejová J., Keckes J., Pálková H. & Komadel P. (2002) Identification of components in smectite/kaolinite mixtures. *Clay Minerals*, **37**, 377–388.

Meier L.P. & Kahr G. (1999) Determination of the cation exchange capacity (CEC) of clay minerals using the complexes of copper(II) ion with triethylenetetramine and tetraethylenepentamine. *Clays and Clay Minerals*, **47**, 386–388.

Miller B.L., Fraser D.M., Miller R.L. *et al.* (1941) Lehigh County Pennsylvania. Pennsylvania Geological Survey, 4th series. County Report **39**, p. 340.

Mills S.J., Kampf A.R., Sejkora J., Adams P.M., Birch W. D. & Plášil J. (2011) Iangreyite: a new secondary phosphate mineral closely related to perhamite. *Mineralogical Magazine*, **75**, 327–336.

Mills S.J., Sejkora J., Kampf A.R., Grey I.E., Bastow T.J., Ball N.A., Adams P.M., Raudsepp M. & Cooper M.A. (2012) Krásnoite, the fluorophosphate analogue of perhamite, from the Huber open pit, Czech Republic and the Silver Coin mine, Nevada, USA. *Mineralogical Magazine*, **76**, 625–634.

Mitra R.P. & Sindhu P.S. (1971) Acid character of sauconite: increase in cation exchange capacity on aging in water and the role of Zn^{2+} and Al^{3+} ions. *Clays and CIay Minerals*, **19**, 391–397.

Mondillo N., Boni M., Balassone G. & Villa I.M. (2014) The Yanque Prospect (Peru): from polymetallic Zn-Pb mineralization to a nonsulphide deposit. *Economic Geology*, **109**, 1735–1762.

Petit S., Righi D. & Decarreau A. (2008) Transformation of synthetic Zn-stevensite to Zn-talc induced by the Hofmann-Klemen effect. *Clays and Clay Minerals*, **56**, 645–654.

Rollinson G.K., Andersen J.C., Stickland R.J., Boni M. & Fairhurst R. (2011) Characterisation of supergene non-sulphide zinc deposits using QEMSCAN®. *Minerals Engineering*, **24**, 778–787.

Ross C.S. (1946) Sauconite – A clay mineral of the montmorillonite group. *American Mineralogist*, **31**, 411–424.

Tiller K.G. & Pickering J.G. (1974) The synthesis of zinc silicates at 20°C and atmospheric pressure. *Clays and Clay Minerals*, **22**, 409–416.

Ufer K., Stanjek H., Roth G., Dohrmann R., Kleeberg R. & Kaufhold S. (2008) Quantitative phase analysis of bentonites by the Rietveld method. *Clays and Clay Minerals*, **56**, 272–282.

Vanderburg W.O. (1988) Mines of Humboldt and Pershing Counties. Nevada Publications, Las Vegas (reissue of U.S. Bureau of Mines Information Circular 6995, Reconnaissance of mining districts in Humboldt County, Nevada, 1938).

van der Marel H.W. & Beutelspacher H. (1976) *Atlas of Infrared Spectroscopy of Clay Minerals and their Admixtures.* Elsevier Scientific Publ. Co., Amsterdam, 396 pp.

Vogels R.J.M.J., Kloprogge J.T. & Geus J.W. (2005a) Synthesis and characterization of saponite clays. *American Mineralogist*, **90**, 931–944.

Vogels R.J.M.J., Kloprogge J.T., Geus J.W. & Beers A.W. F. (2005b) Synthesis and characterization of saponite clays: Part 2. Thermal stability. *American Mineralogist* **90**, 945–953.

Wilkins R.W.T. & Ito J. (1967) Infrared spectra of some synthetic talcs. *American Mineralogist*, **52**, 1649–1661.

Yokoyama S., Tamura K., Hatta T., Nemoto S., Watanabe Y. & Yamada H. (2006) Synthesis and characterization of Zn-substituted saponite (sauconite). *Clay Science*, **13**, 75–80.